Supplemental Material
"The smallest stroke: Occlusion of one penetrating vessel leads to infarction and a cognitive deficit" by Andy Y. Shih, Pablo Blinder, Philbert S. Tsai, Beth Friedman, Geoffrey Stanley, Patrick D. Lyden and David Kleinfeld.

Figure S1. Highly localized damage following occlusion of subsurface penetrating vessel branches and capillaries. (a) Three-dimensional reconstruction of tissue volume collected by *in vivo* TPLSM, showing penetrating vessels projecting downward from the pial surface and subsurface branches. **(b)** Vectorization of arterial vasculature with immediate branches of the penetrating arterioles (2^{nd} order arterioles) highlighted in magenta. Capillaries, defined as vessel segments two or more branches away from the penetrating vessel trunk, were excluded from the vectorization for clarity. **(c)** Vectorization of venular vasculature with immediate branches of the penetrating venules (2^{nd} order venules) highlighted in cyan. In this representative example, second order venules outnumber 2^{nd} order arterioles roughly two to one. **(d)** Microvessel RBC velocity plotted as a function of lumen diameter. Deep microvessel data previously grouped in **Figure 2b** is now segregated into capillaries, and 2^{nd} order penetrating arteriole and penetrating venule branches. The diagonal lines correspond to constant RBC volume flux. **(e)** High-resolution confocal image of tissue damage resulting from occlusion of a single 2^{nd} order penetrating arteriole, as visualized 2 days post-occlusion. Propidium iodide is used to identify necrotic neurons with compromised plasma membranes. As with **Figure 4c**, local endothelial fluorescein-dextran retention was used as a fiducial for re-locating the disrupted vessel during histology. **(f)** Confocal image of tissue damage resulting from occlusion of a single capillary. Note the lack of propidium iodide labeling.

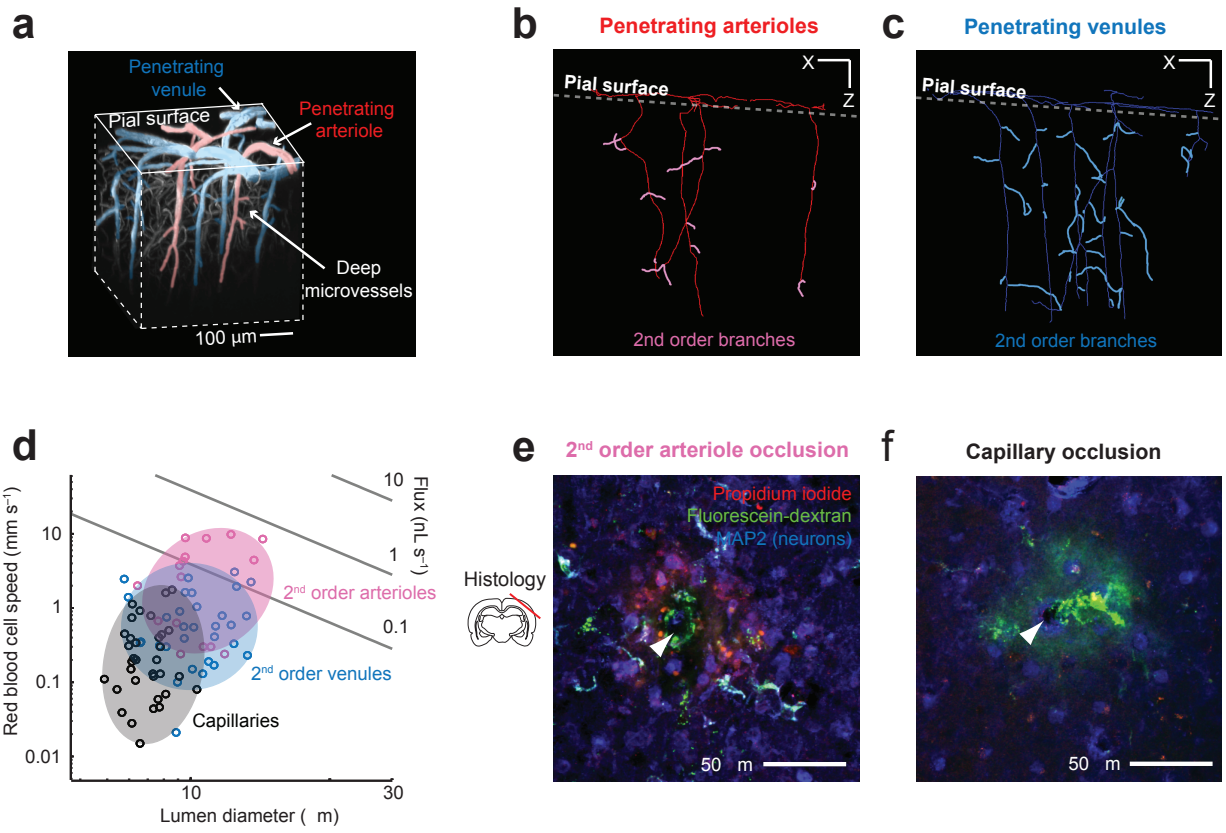

Figure S1. Shih, Blinder, Tsai, Friedman, Stanley, Lyden & Kleinfeld

Supplemental Material
"The smallest stroke: Occlusion of one penetrating vessel leads to infarction and a cognitive deficit" by Andy Y. Shih, Pablo Blinder, Philbert S. Tsai, Beth Friedman, Geoffrey Stanley, Patrick D. Lyden and David Kleinfeld.

Figure S2. Immunohistological analysis of arteriolar and venular microinfarcts reveals vascular damage and blood brain barrier disruption. (a to c) α-hypoxyprobe labeling was restricted to the core of isolated microinfarcts resulting from occlusion of either penetrating arterioles or venules (see also **Fig. 3f**). Animals were perfused 6 h post-occlusion. **(d to f)** Labeling by α-3-nitrotyrosine, a marker of nitrosative protein damage, was increased in cells and vessels restricted to the core of microinfarct. **(g to i)** Labeling by α-aquaporin-4, a marker of blood brain barrier integrity, was reduced in the core of the microinfarct. **(j to l)** Labeling by α-rat immunogloblin G, which indicates leakage of endogenous antibodies from the rat vasculature, was prominent in the tissue bordering the microinfarcts.

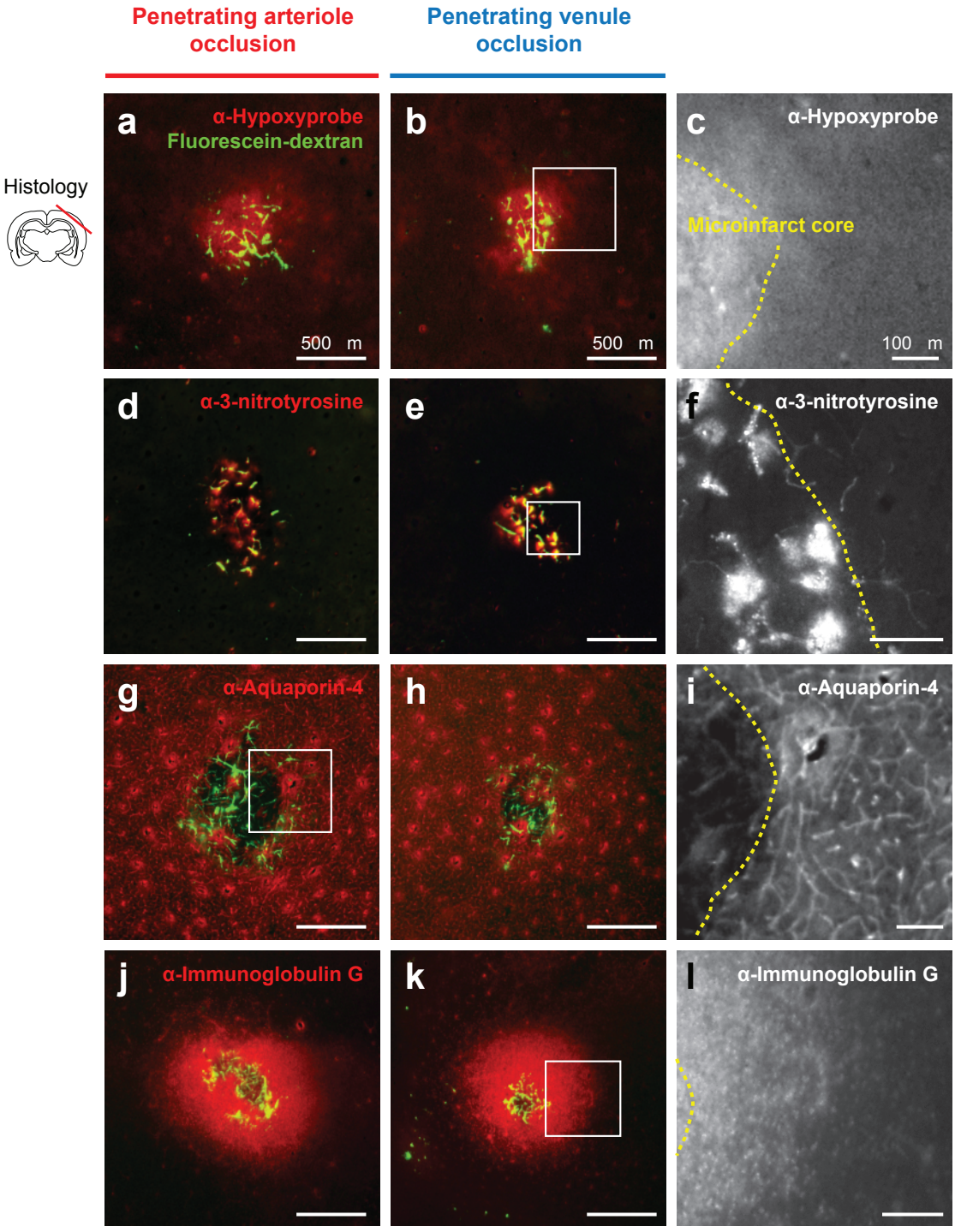

Figure S2. Shih, Blinder, Tsai, Friedman, Stanley, Lyden, Kleinfeld

Supplemental Material
"The smallest stroke: Occlusion of one penetrating vessel leads to infarction and a cognitive deficit" by Andy Y. Shih, Pablo Blinder, Philbert S. Tsai, Beth Friedman, Geoffrey Stanley, Patrick D. Lyden and David Kleinfeld.

Figure S3. Immunohistological analysis of arteriolar and venular microinfarcts reveals necrotic cell death and inflammation in the microinfarct border. (a to c) Propidium iodide-positive neurons, indicative of acute cell death, formed a ring surrounding the microinfarct core (see also **Fig. 3g**). Animals were perfused 6 h post-occlusion. **(d to f)** Labeling by α-CD68, a marker for invading monocytes and macrophages, was increased in the core and border of the microinfarct. **(g to i)** Labeling by α-Iba1, a marker for resident microglia, was reduced within the microinfarct core. A wall of extended microglial processes delineated the immediate boundary of the core.

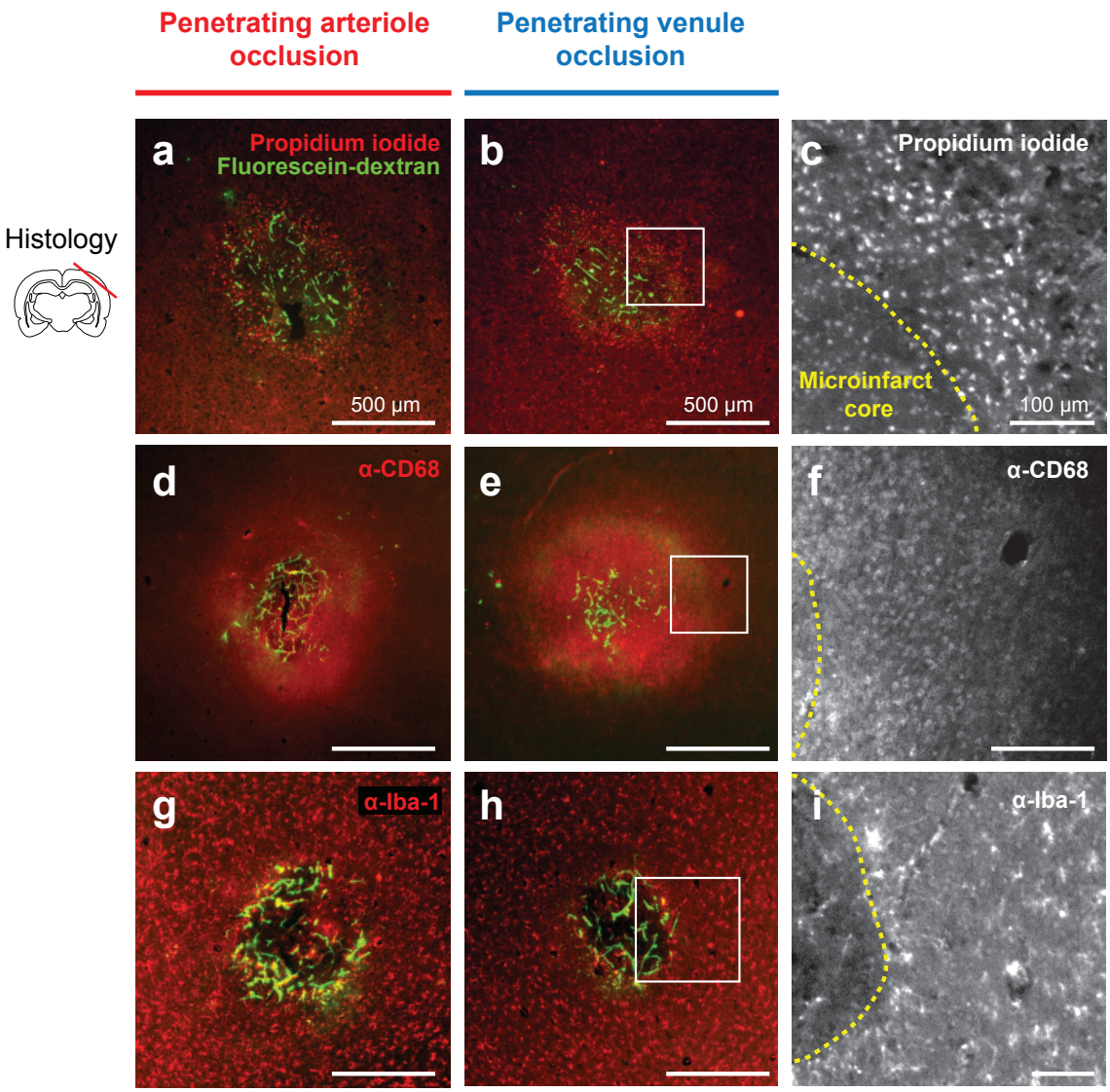

Figure S3. Shih, Blinder, Tsai, Friedman, Stanley, Lyden & Kleinfeld

Supplemental Material
"The smallest stroke: Occlusion of one penetrating vessel leads to infarction and a cognitive deficit" by Andy Y. Shih, Pablo Blinder, Philbert S. Tsai, Beth Friedman, Geoffrey Stanley, Patrick D. Lyden and David Kleinfeld.

Figure S4. Cortical damage induced by penetrating arteriole and penetrating venule occlusions. **(a)** High-magnification views of a 7 day old microinfarct generated by penetrating arteriole occlusion (see also **Fig. 1b & 4a**). The area of tissue damage was delineated as the boundary between viable neuronal NeuN-positive nuclei and regions devoid of nuclei (upper panel; yellow dotted line). Strong NeuN staining in the central region of the microinfarct core is non-specific. GFAP-positive fibers, indicative of astrogliosis, was prevalent in the periphery of the microinfarct and within the immediate boundaries of the core. **(b)** High-magnification views of a 7 day old microinfarct generated by penetrating venule occlusion (see also **Fig. 4b**). Staining features were essentially identical to microinfarcts generated by penetrating arteriole occlusion. **(c)** Examination of a microinfarct seven days after occlusion of a single penetrating arteriole using NeuroTrace™, a fluorescent-based Nissl stain. The inset image shows a magnified view of the brain section. Note the dense labeling within the core, indicating astrogliosis and severe inflammation, typical of a subacute microinfarct. **(d)** Examination of a venular-based microinfarct 7 days after occlusion exhibited similar pathology in the microinfarct core.

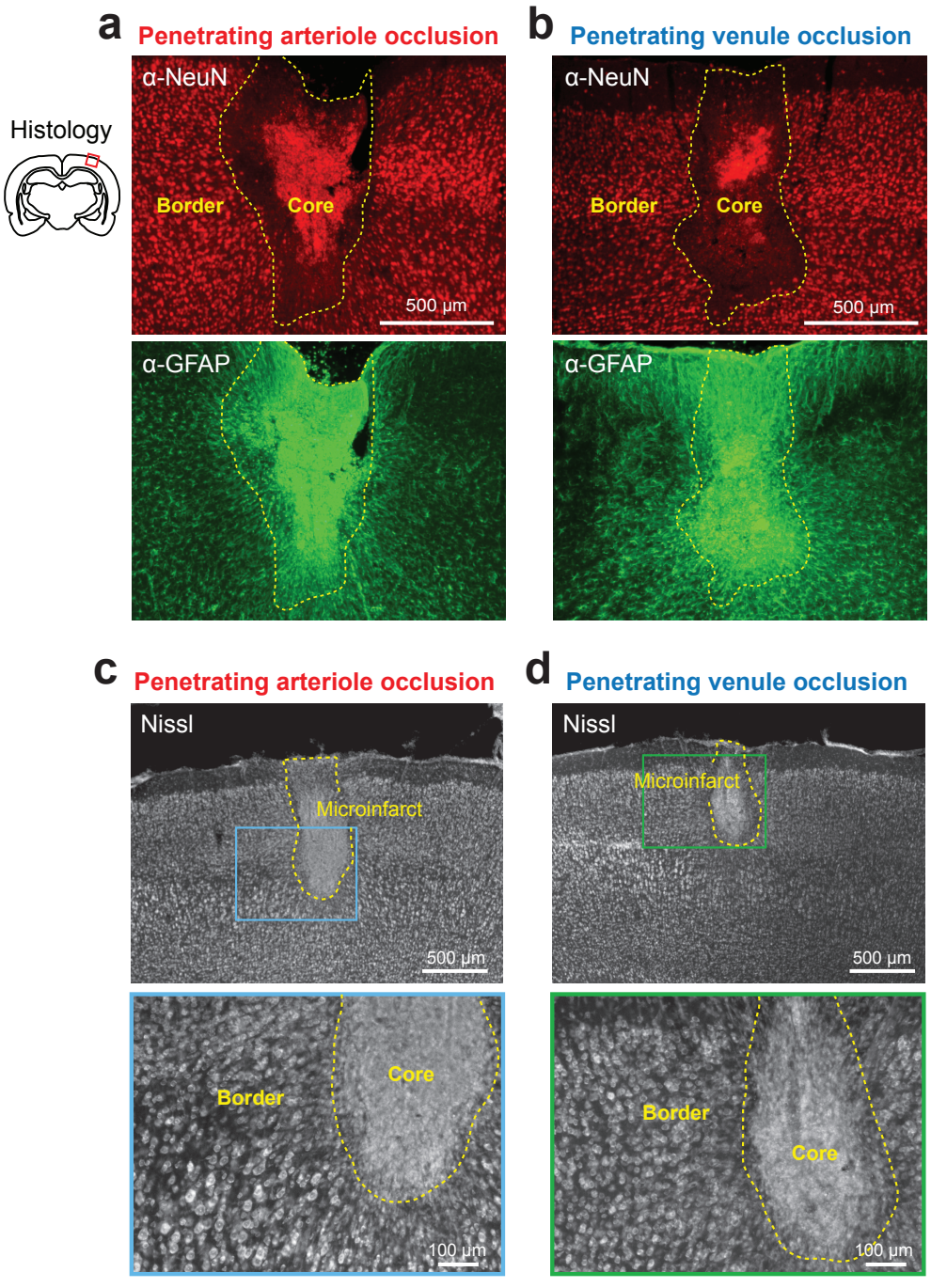

Figure S4. Shih, Blinder, Tsai, Friedman, Stanley, Lyden & Kleinfeld

Supplemental Material
"The smallest stroke: Occlusion of one penetrating vessel leads to infarction and a cognitive deficit" by Andy Y. Shih, Pablo Blinder, Philbert S. Tsai, Beth Friedman, Geoffrey Stanley, Patrick D. Lyden and David Kleinfeld.

Figure S5. Photothrombotic targeting of individual vibrissa columns in vS1 cortex of gap-crossing rats. (a) A Long Evans rat trained for the gap-crossing paradigm was anesthetized with isoflurane and a cranial window was generated over the vibrissa area of somatosensory cortex. The last remaining untrimmed vibrissa, C2, was stimulated with a piezoelectric actuator and the corresponding vibrissa column in the primary vibrissa region of the somatosensory cortex was mapped by intrinsic optical imaging. The stubs of two previously trimmed neighboring vibrissa, in this case, C1 and D2, were also mapped. **(b)** The intrinsic signal was obtained as the reflectance at 630 nm as a function of time while the C2 vibrissa was deflected with a piezoelectric actuator. The dark declivity indicates reduced reflectance, suggesting an increase of deoxygenated hemoglobin and thus increased neural activity in that region. **(c)** To estimate the orientation of the primary vibrissa field *in vivo*, a canonical map of the vibrissa columns was placed atop an image of the pial vasculature, collected with 475 nm light. The vessels within this image were used as fiduciaries for relocation of the column during TPLSM. **(d)** The pial architecture was mapped with greater resolution using TPLSM, and the location of individual penetrating arterioles and venules feeding the target vibrissa column were identified in 3-dimensional image stacks. See inset in panel g. **(e and f)** In this case, a penetrating arteriole did not directly overlap the target vibrissa column (red circles). Rather, a single penetrating venule optimally overlaid the C2 vibrissa representation (blue circles). **(g)** The identified penetrating venule was photothrombotically occluded. A green circle marks the focus of the green laser (upper panel), and a yellow arrow marks the resulting intravascular thrombus (lower panel). **(h)** Following completion of the behavioral experiments, the cortex was examined histologically. The location of the microinfarct was ascertained by α-VGLUT2 staining, while the microinfarct volume was assessed using α-NeuN staining.

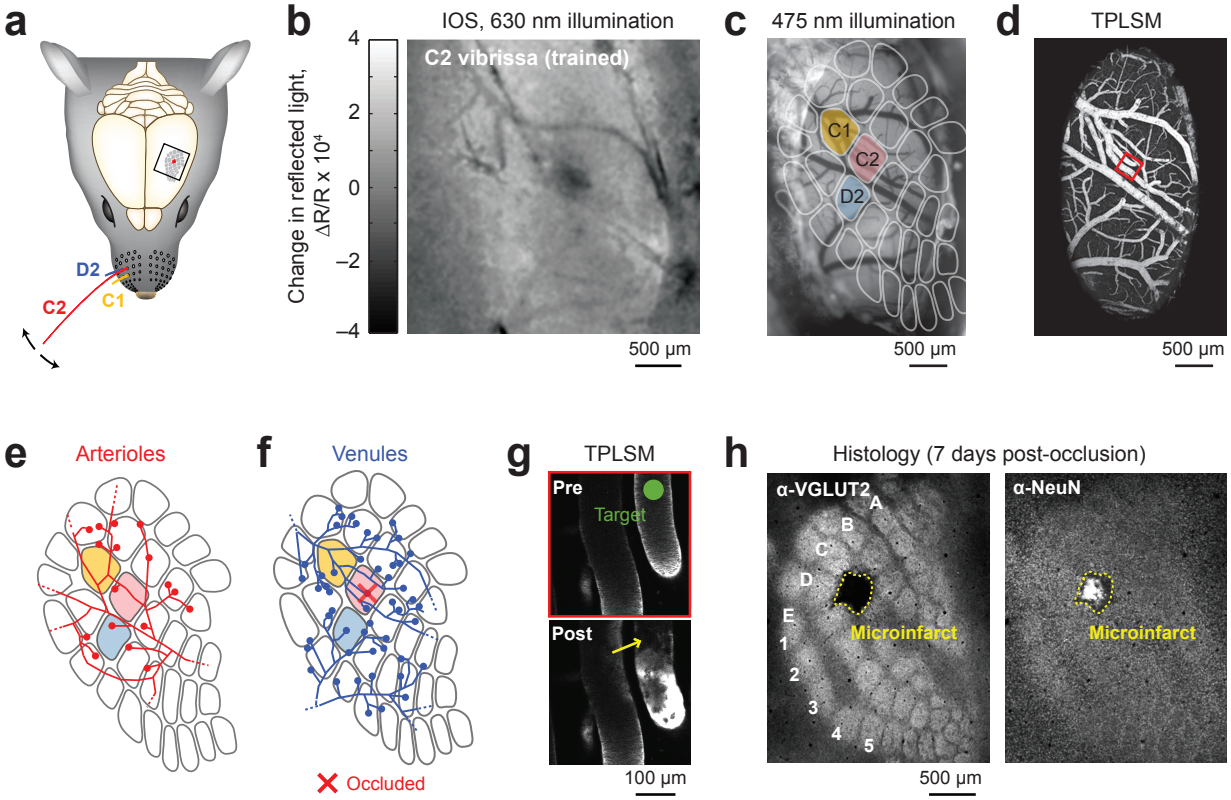

Figure S5. Shih, Blinder, Tsai, Friedman, Stanley, Lyden & Kleinfeld

Supplemental Material
"The smallest stroke: Occlusion of one penetrating vessel leads to infarction and a cognitive deficit" by Andy Y. Shih, Pablo Blinder, Philbert S. Tsai, Beth Friedman, Geoffrey Stanley, Patrick D. Lyden and David Kleinfeld.

Figure S6. Propagation of pial vessel stagnation during microinfarct coalescence revealed by longitudinal imaging. (a) Wide-field view of fluorescein-dextran labeled vasculature as imaged by *in vivo* TPLSM. Penetrating vessels originally targeted for occlusion are marked with yellow circles. High-magnification images of vessels of interest are marked with colored squares (see panel b). Red coloring indicates all vessels that were non-flowing at t = +48h post-occlusion of targeted vessels. Note that the majority of intervening vessels between occlusions become stagnant post-occlusion (see also **Fig. 8c**). A = anterior, M = medial. **(b)** Gradual loss of flow in intervening penetrating vessels. The two upper rows show penetrating venules. The third row shows a non-flowing penetrating arteriole. Yellow arrows highlight stagnant red blood cells within the lumen. The fourth row shows a cluster of penetrating venules, distant from the originally targeted vessels, which retain flow over the time-course of the experiment.

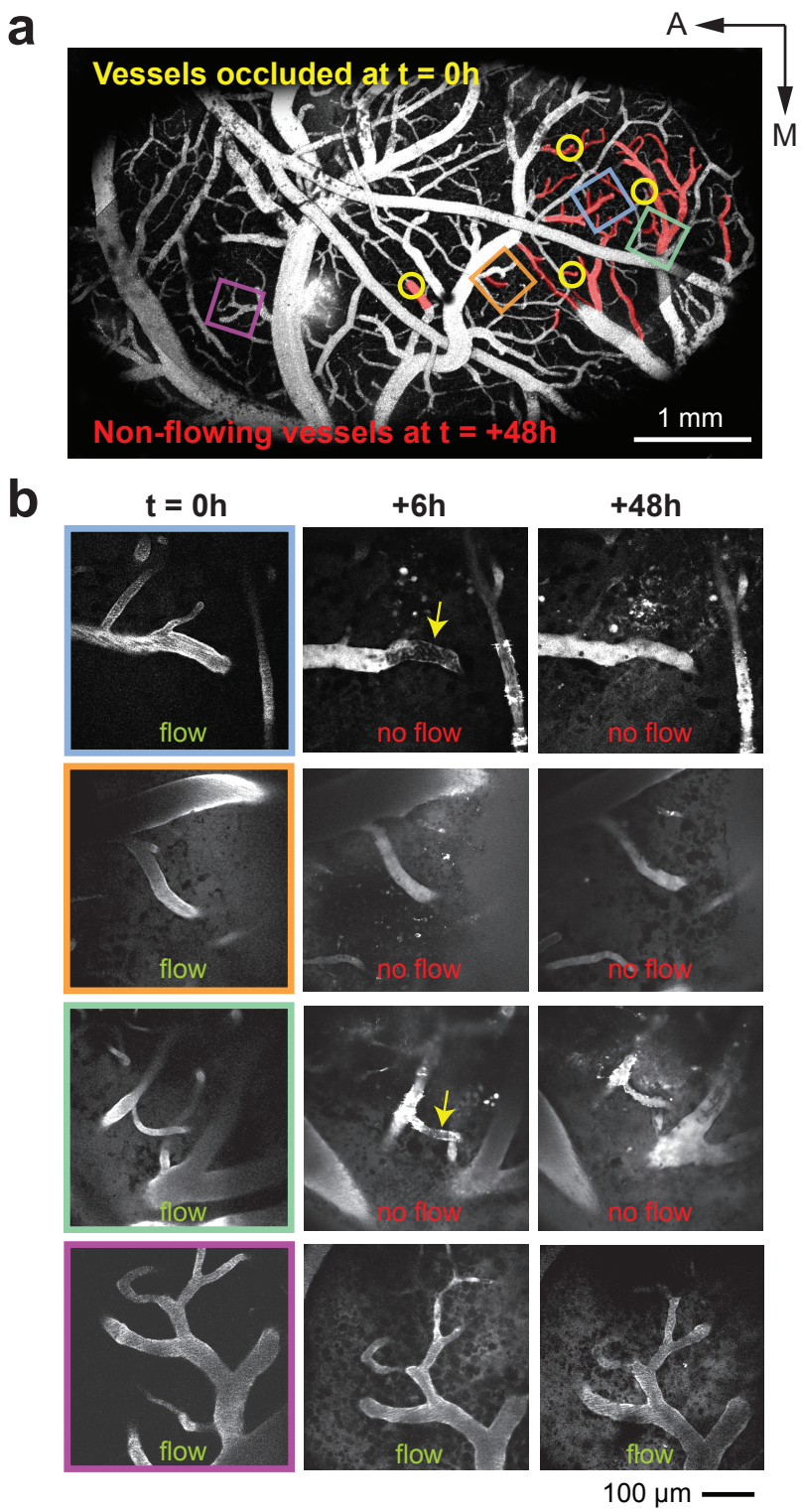

Figure S6. Shih, Blinder, Tsai, Friedman, Stanley, Lyden & Kleinfeld

Supplemental Material
"The smallest stroke: Occlusion of one penetrating vessel leads to infarction and a cognitive deficit" by Andy Y. Shih, Pablo Blinder, Philbert S. Tsai, Beth Friedman, Geoffrey Stanley, Patrick D. Lyden and David Kleinfeld.

Figure S7. Clotting and nitrosative/oxidative damage of microvessels during the process of microinfarct coalescence. (a) Wide-field view of vasculature as imaged by TPLSM. The locations of occluded vessels are marked with a blue circle, with the area of the circle approximating the predicted microinfarct area, based on studies of isolated penetrating vessel occlusions. Three penetrating arterioles were occluded in this example. **(b)** Maximal *in vivo* TPLSM projection of deep microvessels (100 μm below the pia) within the region of coalescence (red arrow in panel a) at early and late stages post-occlusion. Microbleeds (red arrowheads) and occluded lumina (yellow arrowhead) were evident in the microvasculature 24 h post-occlusion. **(c and d)** Histological examination of the microinfarction at 24 h post-occlusion. Two microinfarcts had already coalesced, and a third, more distant microinfarct on the left was in the process of coalescence. The tissue bridging the separate microinfarcts exhibited extensive vascular damage, as evidenced by endothelial fluorescein-dextran retention and strong labeling with α-3-nitrotyrosine.

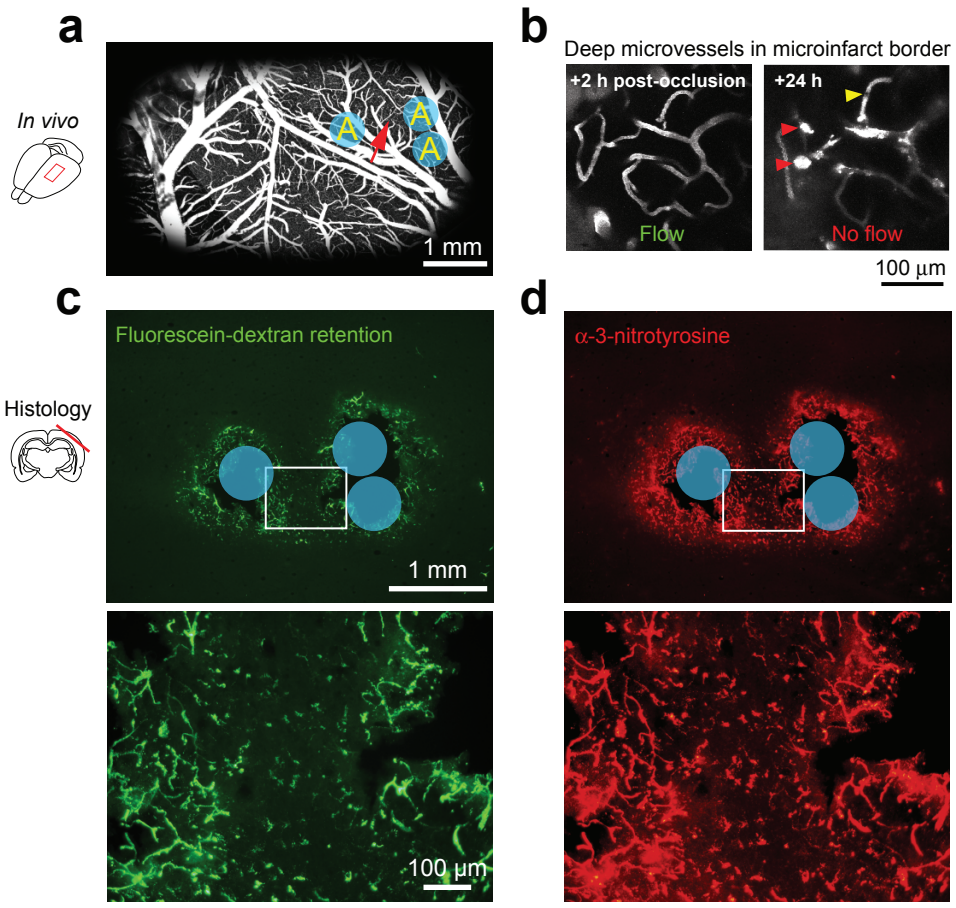

Figure S7. Shih, Blinder, Tsai, Friedman, Stanley, Lyden & Kleinfeld

Supplemental Material
"The smallest stroke: Occlusion of one penetrating vessel leads to infarction and a cognitive deficit" by Andy Y. Shih, Pablo Blinder, Philbert S. Tsai, Beth Friedman, Geoffrey Stanley, Patrick D. Lyden and David Kleinfeld.

Figure S8. Longitudinal imaging of pial vessel flux during microinfarct coalescence and the effect of MK-801. (a) Wide-field view of vasculature as imaged by *in vivo* TPLSM. Vessels that are not flowing at the indicated post-occlusion time-points are shown in red (see also **Figs. 8c & S6**). Four penetrating vessels were initially occluded by photothrombosis (yellow circles). Over the course of 6 to 48 h, flow in intervening vessels, including penetrating vessels completely stagnated. **(b)** In a second animal, the administration of a single bolus of MK-801 at 30 min pre-occlusion prevented the accumulation of stagnated vessels. At 24 h post-occlusion, some photothrombotically target penetrating vessels were found to be re-cannulated (see also **Fig. 8d for chronic effects)**. **(c and d)** Schematic showing the location of repeatedly measured vessels overlaid on the eventual area of tissue damage. **(e and f)** Flux of pial vessels within and outside the region of coalescence in the normal and drug-treated rats.

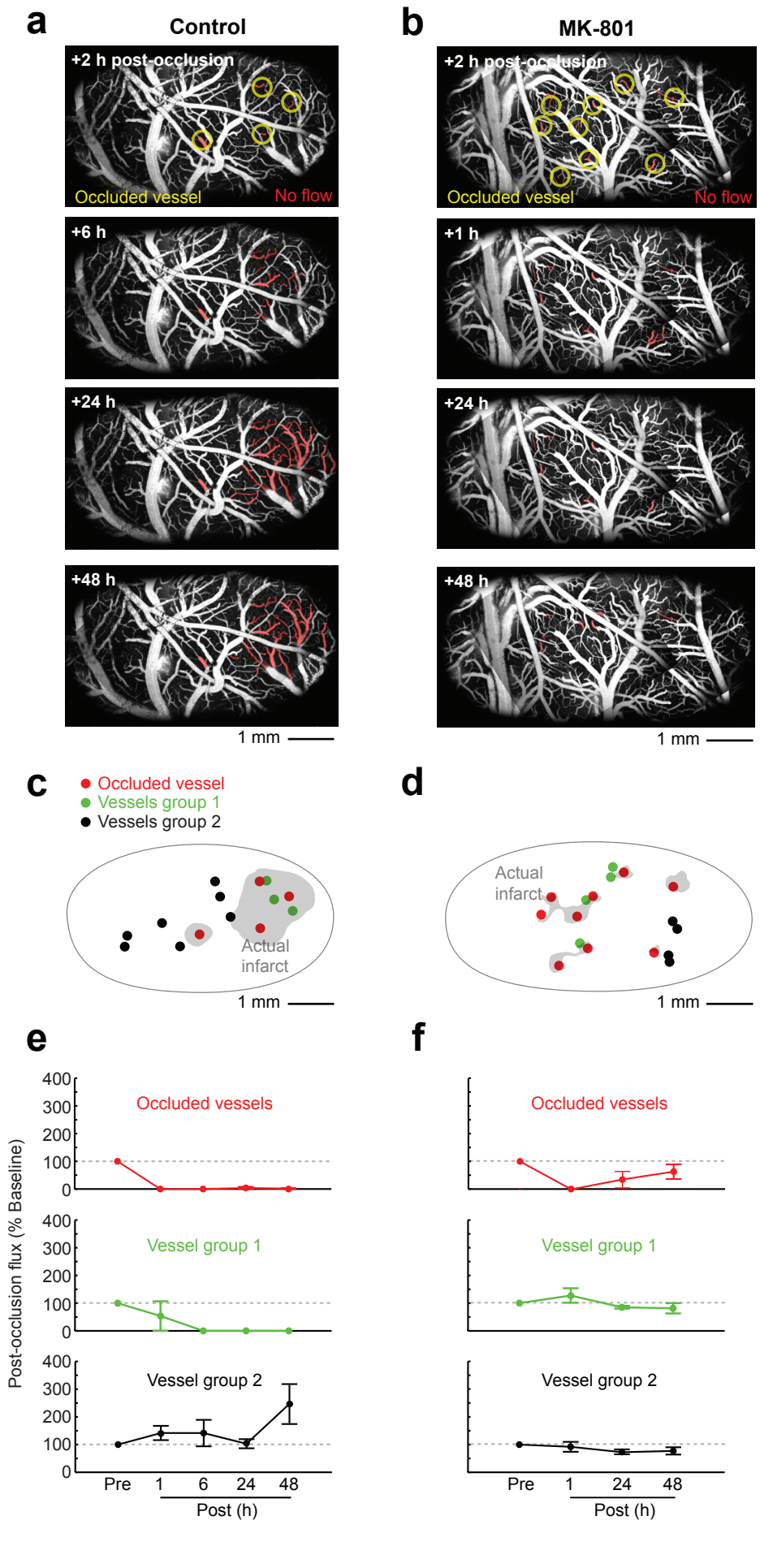

Figure S8. Shih, Blinder, Tsai, Friedman, Stanley, Lyden & Kleinfeld

Supplemental Material
"The smallest stroke: Occlusion of one penetrating vessel leads to infarction and a cognitive deficit" by Andy Y. Shih, Pablo Blinder, Philbert S. Tsai, Beth Friedman, Geoffrey Stanley, Patrick D. Lyden and David Kleinfeld.

Table S1. Inter-group comparison of parameters in gap cross task experiments.

	ON-target microinfarct	**ON-target microinfarct plus Memantine**	**OFF-target microinfarct**
Sample size	10	7	3
Microinfarct-induced change in gap (cm)	-0.8 ± 0.1	-0.3 ± 0.1 *	0 ± 0.1 **
No vibrissa-induced change in gap (cm)	-1.1 ± 0.1	-1.0 ± 0.1	-1.3 ± 0.5
Total microinfarct volume (nL)	272 ± 59	36 ± 11 **	271 ± 74
Volume fraction of cortical column affected	0.28 ± 0.04	0.05 ± 0.01 ***	0 **
Pre-occlusion flux of target vessel (nL/s)	3.4 ± 0.6	3.1 ± 0.8	4.2 ± 2.2

Data presented as mean ± s.e.m., with significance notes as *p<0.05, **p<0.01,and ***p<0.001, as compared to ON-target microinfarct. Statistics were performed with the Kruskal Wallis test and a Dunn's *post hoc* analysis.

Supplemental Material
"The smallest stroke: Occlusion of one penetrating vessel leads to infarction and a cognitive deficit" by Andy Y. Shih, Pablo Blinder, Philbert S. Tsai, Beth Friedman, Geoffrey Stanley, Patrick D. Lyden and David Kleinfeld.

Table S2. Physiological variables for drug studies.

	Pre-occlusion			Post-occlusion		
	Normal (n = 7)	MK-801 (n = 3)	Memantine (n = 6)	Normal	MK-801*	Memantine*
pH	7.35 ± 0.04	7.36 ± 0.07	7.34 ± 0.06	7.34 ± 0.03	7.31 ± 0.06	7.34 ± 0.04
pO_2 (mm Hg)	118 ± 14	106 ± 18	135 ± 14	118 ± 13	112 ± 20	131 ± 19
pCO_2 (mm Hg)	34 ± 4	35 ± 2	32 ± 6	34 ± 3	34 ± 2	33 ± 6
MAP (mm Hg)	93 ± 7	102 ± 7	98 ± 9	95 ± 6	96 ± 4	96 ± 9

Physiological variables measured from animals used in Figure 8f,g. *Variables measured after drug administration. Data is presented as mean ± s.d. MAP = mean arterial blood pressure. Paired t-test was used to compare pre- and post-occlusion values for each physiological variable in each drug treatment group. No significant differences were detected at an alpha level of 0.05.

Supplemental Material
"The smallest stroke: Occlusion of one penetrating vessel leads to infarction and a cognitive deficit" by Andy Y. Shih, Pablo Blinder, Philbert S. Tsai, Beth Friedman, Geoffrey Stanley, Patrick D. Lyden and David Kleinfeld.

Table S3. Summary of primary and secondary antibodies.

Primary antibody	**Species**	**Working dilution**	**Source**
3-nitrotyrosine	Rabbit	1:200	Invitrogen; A21285
AQP4	Rabbit	1:200	Millipore; AB2218
CD68	Mouse	1:100	AbD Serotec; MCA341R
GFAP	Rabbit	1:200	Invitrogen; 18-0063
Hypoxyprobe	Mouse	1:500	Hypoxyprobe.com
Iba1	Rabbit	1:500	Wako; 019-19741
IgG-Cy3	Rat	1:200	Millipore; AB2251
NeuN	Mouse	1:200	Millipore; MAB377
VGLUT2	Guinea Pig	1:12,000	Millipore; AB2251
Secondary antibody	**Species**	**Working dilution**	**Source**
Anti-mouse Alexa 594	Goat	1:1,000	Invitrogen; A31624
Anti-rabbit Alexa 488	Goat	1:1,000	Invitrogen; A31620
Anti-guinea pig Alexa 594	Goat	1:1,000	Invitrogen; A11076